ENaC isn't ASIC

A Study of Various Activating Mutations and Conditions of the Epithelial Sodium Channel

Richard Posert

2023-07-21

Table of contents

Frontmatter

Acknowledgements

We'll get here.

Part I.

Introduction

1. ENaC in the Body

1.1. ENaC in the kidney

Blood pressure must be maintained within a narrow window of acceptable values. Too low, and vital organs do not receive sufficient oxygen and nutrients to function, but too high and blood vessels sustain damage. It is not surprising, then, that the human body has evolved several mechanisms for responding to changes in blood pressure, each with their own timescale[1]. ENaC is the essential mechanism of the longest-term control, kidney excretion.

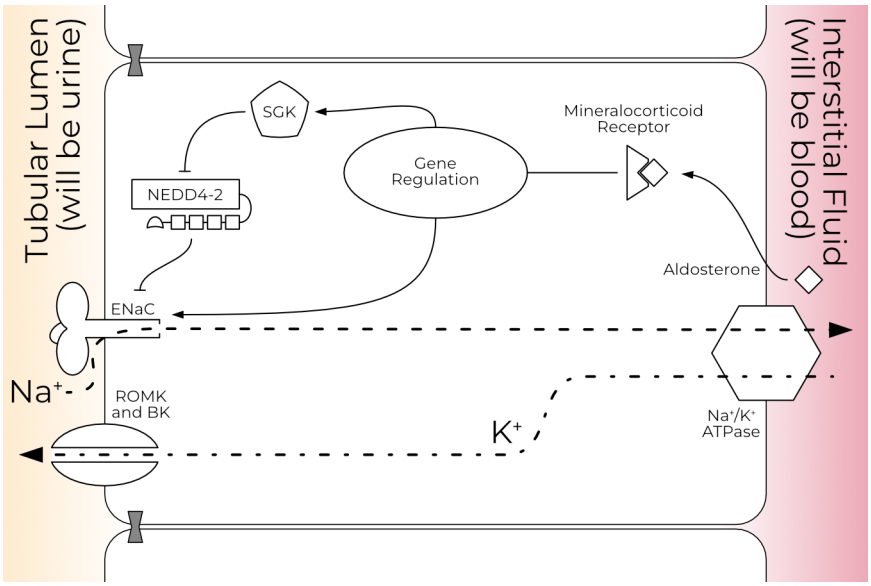

Figure 1.1.: Simplified model of ENaC regulation in a principal cell of the distal nephron in the kidney.

When the kidney is not receiving enough salt, it initiates a cascade which ends with the mineralocorticoid hormone aldosterone augmenting the activity of ENaC in the distal nephron (Figure 1.1). Apical sodium permeability is

Of note: Asher and colleagues report an aldosterone mediated increase in expression of the β and γ, but not α, subunits. A trend of subunit-specific regulation is widely observed in the literature, but poorly understood.

increased both by synthesis of new channels as well as trafficking of an existing pool of channels to the cell surface[2,3]. Despite its expression relatively late in the nephron, ENaC is the rate-limiting step of sodium reabsorption in the kidney. Sodium in the principal cells is transported across the basolateral membrane by the Na^+/K^+ ATPase, and therefore induces retention of extra water to maintain the tightly-controlled plasma sodium level. Thus, ENaC controls three essential functions of kidney filtration: first, the amount of sodium reabsorbed by the kidney; second, blood volume (and therefore pressure); third, the amount of potassium passed from the plasma into the urine.

A variety of ENaC mutations have dramatic effects on patients' blood pressure. One of the earliest described is Liddle syndrome[4]. Liddle syndrome (also called pseudoaldosteronism) results from an autosomal dominant gain-of-function mutation in ENaC. Severe hypertension, low potassium, high blood pH, low renin activity, and low aldosterone are hallmarks of the disease[5]. It is a rare disorder, with only 72 families described as of 2018[6]. However, after excluding patients with other clear causes (primary aldosteronism, kidney or heart diseases, and obstructive sleep apnea), approximately one in one hundred hypertensive patients had Liddle syndrome, indicating that the prevalence may be higher than is currently thought[7,8]. All but one of the described cases involve mutation of the β or γ subunits[6,8].

A majority of the mutations in the β and γ subunits disrupt or remove entirely a proline-rich PY motif at the C-terminus of those channels[9]. This PY motif is the binding site for the E3 ubiquitin ligase NEDD4-2 (see section). Study of ENaC surface dwell time is complicated by a reserve pool maintained by the cells to be cycled up to the membrane, but there is a consensus that ENaC is recycled quickly; surface half life estimates range from fifteen minutes to three hours, with the low end having more support[10]. ENaC lacking the PY motif cannot be pulled back in from the membrane, thus increasing sodium permeability by increasing *N* rather than the conductivity or P_O of the channels[11--13].The α subunit does have a PY motif, but no Liddle syndrome mutation of the α PY has been described. This is discussed further in]{.aside} The remaining minority of described Liddle syndrome mutations (including the sole $ENaC_\alpha$ mutation) which do not affect PY-motif binding instead directly augment channel P_O[6]. Liddle syndrome is typically treated with small molecules that block ENaC (amiloride or triamterene) and a low-salt diet.

Loss-of-function mutations also cause severe phenotypes. Type 1 pseudohypoaldosteronism (PHA1) was first described in a severely dehydrated infant who did not respond to aldosterone treatment[14]. There are two forms of

PHA1: renal PHA1, which is milder and involves a mutation in the mineralocorticoid receptor; and systemic PHA1, which involves a mutation in a gene for ENaC α, β, or γ[15,16]. Patients with systemic PHA1 are unable to retain any salt, and so become severely dehydrated and have high potassium, low sodium, and increased acidity in their blood[5]. This makes the disease particularly deadly to newborns, and requires life-long supplementation with sodium and the potassium elimination drug Kayexalate[17]. Contrary to the pattern observed for Liddle Syndrome, most systemic PHA1 mutations occur in the gene encoding $ENaC_{\alpha}$[17]. The majority of described PHA1 mutations are nonsense mutations, although three missense mutations have been described[16–18]. One of these mutations occurs in the palm domain, one in the transmembrane domain, and one likely in the intracellular domain.

Although the genes for the β and γ subunits are both on chromosome 16 and the gene for $ENaC_{\alpha}$ is on chromosome 12, no difference in the rates of mutation for the affected genes are seen between patients and control groups[17].

References

1. Guyton, A. C. Blood Pressure Control---Special Role of the Kidneys and Body Fluids. *Science* **252**, 1813--1816 (1991).
2. Asher, C., Wald, H., Rossier, B. C. & Garty, H. Aldosterone-induced increase in the abundance of Na+ channel subunits. *American Journal of Physiology-Cell Physiology* **271**, C605--C611 (1996).
3. Frindt, G. & Palmer, L. G. Surface expression of sodium channels and transporters in rat kidney: Effects of dietary sodium. *Am. J. Physiol. Renal Physiol.* **297**, F1249--F1255 (2009).
4. Liddle, G. W., Bledsoe, T. & Coppage, W. S. A familial renal disorder simulating primary aldosteronism but with negligible aldosterone secretion. *Trans. Assoc. Am. Physicians* **76**, 199--213 (1963).
5. Hanukoglu, I. & Hanukoglu, A. Epithelial sodium channel (ENaC) family: Phylogeny, structure--function, tissue distribution, and associated inherited diseases. *Gene* **579**, 95--132 (2016/04/01/).
6. Tetti, M. *et al.* Liddle Syndrome: Review of the Literature and Description of a New Case. *International Journal of Molecular Sciences* **19**, (2018).
7. Wang, L.-P. *et al.* Prevalence of Liddle Syndrome Among Young Hypertension Patients of Undetermined Cause in a Chinese Population. *The Journal of Clinical Hypertension* **17**, 902--907 (2015).
8. Liu, K. *et al.* Analysis of the genes involved in Mendelian forms of low-renin hypertension in Chinese early-onset hypertensive patients. *Journal of Hypertension* **36**, (2018).
9. Yang, K.-Q., Xiao, Y., Tian, T., Gao, L.-G. & Zhou, X.-L. Molecular genetics of Liddle's syndrome. *Clinica Chimica Acta* **436**, 202--206 (2014).
10. Butterworth, M. B., Edinger, R. S., Frizzell, R. A. & Johnson, J. P. Regulation of the epithelial sodium channel by membrane trafficking. *American Journal of Physiology-Renal Physiology* **296**, F10--F24 (2009).

11. Schild, L. *et al.* A mutation in the epithelial sodium channel causing Liddle disease increases channel activity in the Xenopus laevis oocyte expression system. *Proceedings of the National Academy of Sciences* **92**, 5699--5703 (1995).

12. Abriel, H. *et al.* Defective regulation of the epithelial Na+ channel by Nedd4 in Liddle's syndrome. *J Clin Invest* **103**, 667--673 (1999).

13. Lu, C., Pribanic, S., Debonneville, A., Jiang, C. & Rotin, D. The PY Motif of ENaC, Mutated in Liddle Syndrome, Regulates Channel Internalization, Sorting and Mobilization from Subapical Pool. *Traffic* **8**, 1246--1264 (2007).

14. CHEEK, D. B. & PERRY, J. W. A salt wasting syndrome in infancy. *Arch Dis Child* **33**, 252--256 (1958).

15. Geller, D. S. *et al.* Mutations in the mineralocorticoid receptor gene cause autosomal dominant pseudohypoaldosteronism type I. *Nature Genetics* **19**, 279--281 (1998).

16. Chang, S. S. *et al.* Mutations in subunits of the epithelial sodium channel cause salt wasting with hyperkalaemic acidosis, pseudohypoaldosteronism type 1. *Nature Genetics* **12**, 248--253 (1996).

17. Edelheit, O. *et al.* Novel mutations in epithelial sodium channel (ENaC) subunit genes and phenotypic expression of multisystem pseudohypoaldosteronism. *Clinical Endocrinology* **62**, 547--553 (2005).

18. Schaedel, C. *et al.* Lung symptoms in pseudohypoaldosteronism type 1 are associated with deficiency of the α-subunit of the epithelial sodium channel. *The Journal of Pediatrics* **135**, 739--745 (1999).

19. Kawate, T. & Gouaux, E. Fluorescence-Detection Size-Exclusion Chromatography for Precrystallization Screening of Integral Membrane Proteins. *Structure* **14**, 673--681 (2006/04/01/).

20. Noreng, S., Bharadwaj, A., Posert, R., Yoshioka, C. & Baconguis, I. Structure of the human epithelial sodium channel by cryo-electron microscopy. *eLife* **7**, e39340 (2018).

21. Noreng, S., Posert, R., Bharadwaj, A., Houser, A. & Baconguis, I. Molecular principles of assembly, activation, and inhibition in epithelial sodium channel. *eLife* **9**, e59038 (2020).

22. Mastronarde, D. N. SerialEM: A Program for Automated Tilt Series Acquisition on Tecnai Microscopes Using Prediction of Specimen Position. *Microscopy and Microanalysis* **9**, 1182--1183 (2003).

23. Jumper, J. *et al.* Highly accurate protein structure prediction with AlphaFold. *Nature* **596**, 583--589 (2021).

24. Croll, T. ISOLDE: A physically realistic environment for model building into low-resolution electron-density maps. *Acta Crystallographica Section D* **74**, 519--530 (2018).

25. Pettersen, E. F. *et al.* UCSF ChimeraX: Structure visualization for researchers, educators, and developers. *Protein Sci* **30**, 70--82 (2021).

26. Emsley, P., Lohkamp, B., Scott, W. G. & Cowtan, K. Features and development of Coot. *Acta Crystallographica Section D* **66**, 486--501 (2010).

27. Liebschner, D. *et al.* Macromolecular structure determination using X-rays, neutrons and electrons: Recent developments in Phenix. *Acta Crystallographica Section D* **75**, 861--877 (2019).

28. Williams, C. J. *et al.* MolProbity: More and better reference data for improved all-atom structure validation. *Protein Science* **27**, 293--315 (2018).

29. Pintilie, G. *et al.* Measurement of atom resolvability in cryo-EM maps with Q-scores. *Nature Methods* **17**, 328--334 (2020).

30. Aiyer, S., Zhang, C., Baldwin, P. R. & Lyumkis, D. Evaluating Local and Directional Resolution of Cryo-EMCryo-electron microscopy (Cryo-EM) Density Maps. in *cryoEM: Methods and Protocols* (eds. Gonen, T. & Nannenga, B. L.) 161--187 (Springer US, 2021). doi:10.1007/978-1-0716-0966-8_8.

31. Mukherjee, A. *et al.* Cysteine Palmitoylation of the γ Subunit Has a Dominant Role in Modulating Activity of the Epithelial Sodium Channel*. *J. Biol. Chem.* **289**, 14351--14359 (2014/05/16/).

32. Mueller, G. M. *et al.* Cys Palmitoylation of the Beta Subunit Modulates Gating of the Epithelial Sodium Channel. *J. Biol. Chem.* **285**, 30453--30462 (2010).

33. Mueller, G. M. *et al.* Multiple residues in the distal C terminus of the α-subunit have roles in modulating human epithelial sodium channel activity. *American Journal of Physiology-Renal Physiology* **303**, F220--F228 (2012).

34. Snyder, P. M., Bucher, D. B. & Olson, D. R. Gating Induces a Conformational Change in the Outer Vestibule of Enac. *Journal of General Physiology* **116**, 781--790 (2000).

35. Kashlan, O. B. *et al.* Allosteric inhibition of the epithelial Na+ channel through peptide binding at peripheral finger and thumb domains. *J Biol Chem* **285**, 35216--35223 (2010).

A. Materials and Methods

A.1. ENaC Expression

A.1.1. Human ENaC

Human embryonic kidney cells (HEK293T/17) were grown in suspension in Freestyle medium with 2% FBS at a density of 2 -- 4×10^6 cells/mL. BacMam virus carrying the genes for the appropriate ENaC subunits were added to the flasks at an MOI of 1 and incubated at 37 °C for 8 hours, after which 1 μM amiloride was added and the flasks were moved to 30 °C. After a total incubation time of 72 hours, cultures were centrifuged at 4,790 xg for 20 minutes to collect pellets. The pellets were washed with **TBS** (20 mM Tris pH 8.0, 200 mM NaCl) and centrifuged again before snap-freezing in liquid nitrogen. Cell pellets were stored at -80 °C until use.

A.1.2. Mouse ENaC

Sf9 cells were grown in suspension in Sf900-II serum-free media at 27 °C. Cells were infected at log phase with virus encoding full-length mouse $ENaC_{\alpha}$, $ENaC_{\beta}$, and $ENaC_{\gamma}$. After 5--6 hours of growth, 1 µM amiloride was added to the culture. Cells were harvested 24 hours later, washed with TBS, flash frozen in liquid nitrogen, and stored at -80 °C until used.

A.2. ENaC Purification

A.2.1. Human ENaC

Throughout this protocol, quantities of resin and buffer are given ``per flask''. I grow cell culture in quantities of 800 mL culture per flask, meaning that, e.g., pelleted cells from 1.6 L of cells require twice the quoted quantities of

buffer and resin. In datasets with NaCl listed as the salt, solubilization buffer, wash buffers, elution buffer, and SEC buffer used NaCl in place of KCl.

To purify ENaC, frozen whole-cell pellets were removed from the -80 °C freezer and thawed in a 37 °C water bath. While the pellets were thawing, 50 mL **Solubilization Buffer** was prepared per flask:

- 20 mM Tris pH 7.5, 200 mM KCl
- 1 tablet per 100 mL Pierce EDTA-free protease inhibitor tablets
- 25 U/mL ThermoFisher universal nuclease
- 2.5 mM ATP, 5 mM $MgCl_2$
- 10 mg/mL digitonin
- 10 μM amiloride

The solubilization buffer was prepared fresh at 2X concentration (i.e., half the final volume). Once pellets were fully thawed, they were added to the solubilization buffer and the mixture was brought to the final volume with DI water and poured into a screw-cap bottle. The solubilization mixture was left at 8 °C for 1.5 hours.

After solubilization was complete, the crude lysate was decanted into ultracentrifuge tubes and centrifuged at 100,000 xg for 45 minutes at 4 °C. Meanwhile, in-house-made GFP-nanobody CNBr resin (0.8 mL per flask) was loaded into an XK 16 column and washed with 2 CV of TBK

- 20 mM Tris pH 7.5
- 200 mM KCl

and the following buffers were prepared in the listed quantities:

wash A (10 column volumes [CV]):

- 20 mM Tris pH 7.5, 200 mM KCl
- 0.7 mg/mL digitonin
- 2 mM $MgCl_2$
- 2 mM ATP
- 2 nM phenamil

wash B (10 CV):

- 20 mM Tris pH 7.5
- 200 mM KCl
- 0.7 mg/mL digitonin
- 5 mM $CaCl_2$

- 2 nM phenamil;

elution buffer (5 CV): wash B with 33 μg/mL thrombin

The column was washed with 2 CV of wash A, then clarified lysate was bound to the column under 4 mL/min flow. A small aliquot of pre-column and post-column clarified lysate was reserved to assess binding efficiency by GFP FSEC[19]. If binding efficiency fell below 90% of the initial efficiency the resin was discarded. Otherwise, it was regenerated with pulsed pH cleaning. The GFP-nanobody column was washed with 5 CV wash A and B.

To elute ENaC from the GFP nanobody resin, the column was washed 3 times with 1.5 CV elution buffer and once with TBK + 0.7 mg/mL digitonin. As each wash was flowed on, the eluant was collected in 1 mL or 0.25 CV fractions, whichever was smaller. This results in four sets of fractions: the first comprises largely wash B with little protein (from the initial flow-on of elution buffer), and the remaining three elution buffer. All fractions were run on an SDS-PAGE gel, and fractions with bands at the expected molecular weight for ENaC were pooled and concentrated to a final volume of 0.5 mL. If the preparation was acid-shocked, the protein was desalted into **acid shock** buffer at this stage:

- 20 mM Tris pH 6
- 200 mM KCl
- 0.7 mg/mL digitonin
- 2 nM phenamil

If the preparation required Fabs, they were added in two-fold excess of protein concentration (as determined by nanodrop A_{280}) at this stage. A final concentration of 1 mM C8 PIP_2 was added to the CKO/DEG monofab samples just before grid preparation.

The concentrated eluant was loaded onto a Superose 6 Increase 10/300 column (Cytiva) equilibrated in **SEC buffer** for further purification via SEC.

- 20 mM Tris pH 7.5
- 200 mM KCl
- 0.7 mg/mL digitonin
- 2 nM phenamil

SEC was typically run overnight, meaning fractions remained at 4 °C until the next morning. Fractions from the SEC peak were collected and assayed for purity and monodispersity by SDS-PAGE and tryptophan FSEC. Monodisperse

peaks were pooled and used the same day. Thus, total time between cell pellet thaw and protein use was typically less than 36 hours.

A.2.2. Mouse ENaC

Frozen cell pellet was thawed on ice. Membranes were prepared by sonication and centrifugation, then re-frozen until purification. For each gram of membranes, 15 mL of **solubilization buffer** was added

- 4 mM GDN
- 20 mM HEPES pH 7.6
- 150 mM NaCl
- 2 mM ATP
- 2 mM $MgSO_4$
- 1 mM TCEP
- 100 µM amiloride
- 1 tablet per 100 mL Pierce EDTA-free protease inhibitor tablets

Membrane pellet was mixed thoroughly and homogenized with a Dounce homogenizer. Cell pellet was stirred for 1 hour at 4 °C. Solubilized membranes were centrifuged at 100,000 xg for 45 minutes at 4 °C.

Next, 300 µL GFP nanobody CNBr resin per gram of membrane was loaded into a gravity column and washed with 10 CV **HBS**

- 20 mM HEPES pH 7.6
- 150 mM NaCl)

and 3 CV **wash A**

- 0.1 mg/mL GDN
- 20 mM HEPES pH 7.6
- 150 mM NaCl
- 1 mM TCEP
- 100 nM phenamil

Clarified lysate was flowed over this column under gravity. The column was washed with 6 CV each of wash A, **wash B** (wash A plus 2 mM ATP, 2 mM $MgSO_4$), **wash C** (wash A plus 25 U/mL ThermoFisher Universal Nuclease), and **elution buffer** (wash A plus 5 mM $CaCl_2$). ENaC was eluted by flowing 1 CV of elution buffer plus 30 µg/mL thrombin onto the column and collecting

the supernatant. After an hour, this process was repeated. These elution steps were repeated for a total of four elutions of 1 CV each.

The first three elutions were pooled and concentrated to 0.5 mL. Fab was added at a one-to-one ratio with nominal protein concentration by nanodrop. Sample was incubated for 10 minutes at room temperature, then centrifuged at 100,000 xg for 20 minutes at 4 °C. The clarified sample was loaded onto a Superose 6 Increase 10/300 column (Cytiva) equilibrated in fresh wash A buffer. Fractions were assessed for purity via SDS-PAGE and FSEC before proceeding to grid preparation or other uses.

A.3. ENaC nanodisc preparation

To prepare nanodiscs, 15 mg of a chloroform stock of POPC (Avanti) was dried down under an argon stream. The lipid film was left overnight in a vacuum desiccator to remove all chloroform. The lipids were then resuspended in 350 μL **reconstitution buffer**

- 20 mM HEPES pH 7.4
- 100 mM KCl
- 1 mM EDTA

and sonicated until the solution was milky in appearance and no lipids remained adhered to the sides of the tube, typically 5--10 minutes. To this solution, 150 μL of 350 μM DM in reconstitution buffer was added. The resulting 500 μL suspension was sonicated in 5 minute bursts until completely clear. To this suspension, 1 mL TBS was added to prepare a final lipid concentration of 10 mg/mL.

Lipids, ENaC, and MSP2N2 were mixed at a final MSP:POPC:ENaC molar ratio of 1:31:0.04. The final concentration of MSP2N2 was kept at 100 μM by further concentrating ENaC or adding lipid reconstitution buffer with 35 mM DM as necessary. This reconstitution mixture was incubated at room temperature for 1 hour. During this incubation, biobeads were washed once in 100% methanol, three times in water, and once in TBS. After 90 minutes, 215 mg washed biobeads per 1 mL reconstitution mixture were added. After 1 hour, the reconstitution mixture was moved to a fresh aliquot of equilibrated biobeads and left nutating overnight at room temperature, approximately 16 hours. The reconstitution mixture was pipetted off the biobeads, filtered with a 0.2 μm filter, and purified via SEC using a Superose 6 Increase 10/300 column in TBS. Typical yields were extremely low, between 5--10% of input

ENaC. The protein assembly was stable with minimal aggregation at 4 °C (assessed by cryoEM and SEC) for at least two weeks.

A.4. Western Blots

SDS-PAGE gels were blotted onto nitrocellulose membranes. Membranes were blocked in 50 mg/mL milk in TBST for 1 hour at room temperature. Primary antibody (**ENaC$_\alpha$**: Santa Cruz Biotechnology αENaC (H-95) sc-21012 lot no. L2812; **ENaC$_\gamma$**: abcam Anti-epithelial Sodium Channel gamma ab133430) was added to this same blocking buffer at 10 µg/blot and incubated overnight at 4 °C. Membranes were washed 3 times with TBST for 5 minutes before addition of secondary antibody (LI-COR IRDye 800 CW Goat anti-Mouse 925-32210 lot no. D21115-21) in TBST. Membranes were incubated at room temperature with secondary for 1 hour, washed 3 times with TBST and once with TBS, then imaged (LI-COR Odyssey DLx).

A.5. cryoEM Grid Preparation

Grid preparation different slightly for each dataset, but followed the same general procedure (Table A.1). Purified GFP-cleaved ENaC was concentrated for grid preparation just before blotting and freezing. All grids were glow discharged at 15 mA for 60 seconds on a Pelco easiGlow before blotting. Grids were frozen using a Vitrobot Mark III (Thermo Fisher). Vitrobot parameters were set as follows: blot time 2, wait time 0, drain time 0, blot force 1, humidity 100%, temperature 12 °C. ``Double-blotted" grids had a protein droplet loaded, manually blotted with torn Whatman filter paper, and a fresh droplet loaded onto the grid before Vitrobot blotting (with Vitrobot filter paper rings) and freezing. This double-blotting process typically took approximately five seconds from first drop to plunge-freeze. In all cases, each protein droplet was 3 μL.

Most datasets were collected with at least one of our two pseudosymmetry-breaking Fabs, developed previously[20]. I have switched from using both Fabs to only using one, because the β-binding Fab is more flexible than the α-binding Fab, and this flexibility reduces overall alignment property. Additionally, one of the two human CKO datasets was first incorporated into nanodiscs and solved without any Fabs. As expected based on our previous studies of electrophysiology of the Fab-bound channels, our ECD models

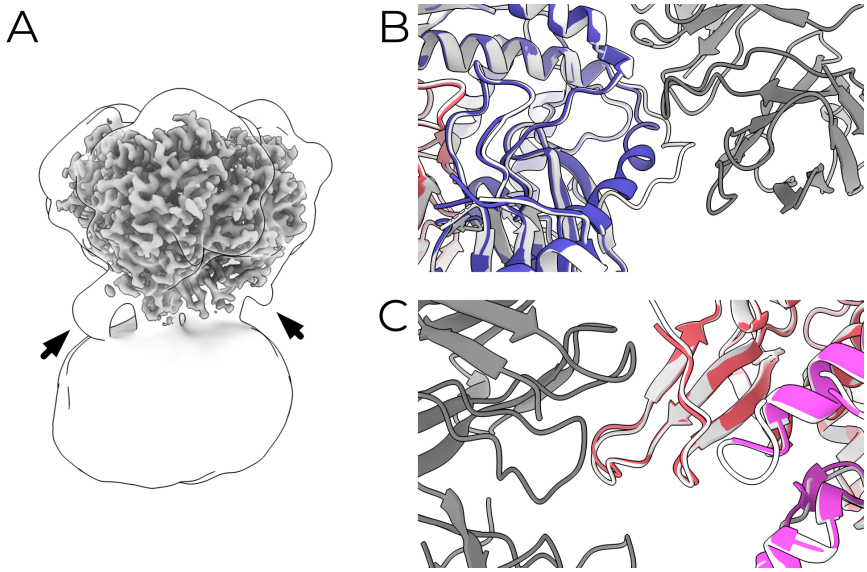

Figure A.1.: Fab binding induces only minor changes in the extracellular domain of ENaC. A: Human CKO/DEG map. A low-pass filtered map is outlined to show pseudosymmetry-breaking glycosylation sites (arrows). B: the α subunit, C: the β subunit. Human CKO nanodisc model is colored by subunit, the human CKO/DEG ENaC is white, and human CKO/DEG Fabs are grey.

with and without Fab are largely indistinguishable (Figure A.1 B,C)[21]. Neither fab significantly distorts the surrounding ECD environment when bound. The α-binding Fab induces a slight shift in a region near the β-ball, while the β-binding Fab induces no detectable change at all.

A.6. cryoEM Data Collection

Datasets were collected using SerialEM by microscopy core staff at the facilities used (Table A.1)[22]. In all cases, multi-shot multi-hole regimes were used to maximize the number of movies recorded. Number of shots per hole and maximum beam shift were a function of ice quality and grid type, but typically a 3x3 pattern of holes was imaged 2--4 times per hole.

A.7. cryoEM Image Processing

Each dataset was processed slightly differently, but following the same general pipeline. First, movies were imported into cryoSPARC for pre-processing. Default parameters were used for both motion correction and CTF estimation. Next, particles were picked using the blob picker in cryoSPARC. Adjustments were made to the minimum and maximum radii to account for the number of Fabs present in each sample. Blob picks for several micrographs were manually inspected and adjusted. First, the NCC parameter was adjusted until few contaminant and carbon-edge picks remained. Next, in a low-defocus micrograph, the low power threshold was adjusted to remove empty ice picks. Finally, in a high-defocus micrograph, the high power threshold was adjusted to remove all carbon-edge and contaminant picks. These initial blob picks were cleaned by 2D classification, and the resulting particle sets used to generate templates for template picking. Template picked thresholds were adjusted as for blob picked particles.

The template picked particles were repeatedly 3D classified using heterogeneous refinement in cryoSPARC, providing one ``good" class and a number of ``junk" classes (typically noisy or bad *ab initio* models of the blob picked particles) until all particles produced reasonable ENaC classes. The final particle set was never 2D classified, since I find that 2D classification reduces the frequency of rare particle views. From this point, processing proceeded *ad hoc* to produce the final maps (Image Processing).

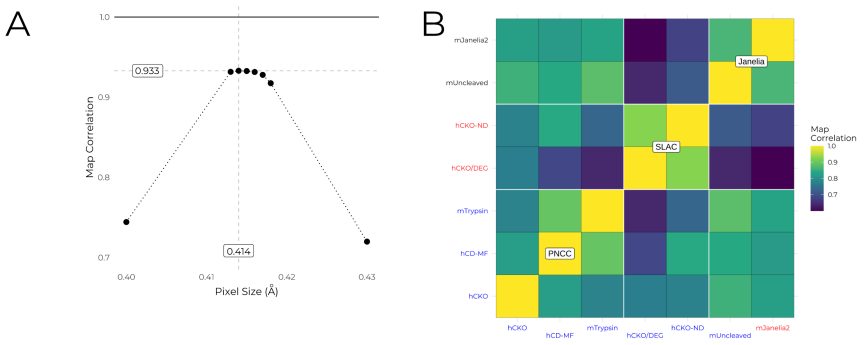

Figure A.2.: S^2C^2 pixel sizes seem miscalibrated. **A**: Scaling the nominal pixel size for human CKO/DEG dramatically increases the correlation with human CKO digitonin. **B**: Correlation coefficients for all maps. Maps were aligned prior to taking correlation coefficients. Abbreviated as follows: hCKO: human CKO; hCD-MF: human CKO/DEG monofab; mTrypsin: trypsin-cleaved mouse; hCKO/DEG: human CKO/DEG difab; hCKO-ND: human CKO nanodisc; mUncleaved: mouse uncleaved; mJanelia2: a second uncleaved mouse dataset collected at Janelia, but not presented here.

During image processing, I began to suspect that the pixel sizes provided by S^2C^2 are likely miscalibrated. First, other users reported pixel size calibration issues with S^2C^2 microscopes around the time these datasets were collected (Patrick Mitchell, S^2C^2 Director of Operations, personal communication). Second, scaling the CKO/DEG difab pixel size from the nominally-correct 0.43 to 0.414 (a change of approximately 3.6%) changes the map correlation value from 0.72 to 0.93 (Figure A.2 A). Finally, a comparison of the correlation between seven recently-collected ENaC maps shows that S^2C^2 is an outlier, with unscaled maps generated from data collected at PNCC and Janelia Farm correlating better with themselves and each other than with those collected at S^2C^2 regardless of construct (Figure A.2 B). I therefore decided to scale both S^2C^2 maps to correlate best with the same condition and construct recorded at PNCC after processing was complete. I present the models built into the scaled maps in this work.

A.8. Model Building

The starting model for mouse ENaC was generated using a local installation of AlphaFold[23]. The amino acid sequences for mENaC α (Uniprot ID Q61180), β (Uniprot ID Q9WU38), and γ (Uniprot ID Q9WU39) were joined using 10xGS linkers between α and β, and β and γ. This meta-sequence was then entered as the AlphaFold target. The linkers and large, unstructured, low-confidence loops were removed from the model before proceeding.

Before docking into experimental maps, starting models had Fabs and waters deleted to ease early model building steps. Initial models were rigid-body fitted into the experimental maps. Any loops in poor or missing regions of the map were deleted. The whole models were simulated with distance restraints using ISOLDE and ChimeraX[24,25]. Once models were roughly fit into the potential, strained distance restraints were released. Once the backbone appeared to fit reasonably well into the map, all distance restraints were released. Simulating one chain at a time, a pass over every residue in ENaC was performed, focusing on Ramachandran values and rotamers. Once all chains had been optimized in this manner, glycans were added using Coot's carbohydrate module[26]. Fabs were rigid-body fitted and simulated similarly to the initial models once these steps were complete.

Models were refined using Phenix real-space refinement[27]. In some cases, the TMD map was used as-is for refinement. In other cases, the ECD and TMD map were combined using Phenix's ``Combine Focused Maps" job and the resulting map was used for refinement. In these cases, the lowest GS-FSC resolution was provided to Phenix. Parameters were left as default, except rotamers were only refined when they had both poor map quality *and* were outliers (rather than *or*). I changed this setting because rotamer and clash statistics were significantly worse if it was left as the default. Model quality was assessed using MolProbity within Phenix, Q-scores calculated in ChimeraX, and 3DFSC as implemented in cryoSPARC (Table A.1 and Model Validation)[28–30].

A.9. Constructs

Table A.1.: Image processing and mod

	human CKO	

	Digitonin	Nanodisc	Difab
Construct Summary			
α mutations	C63A, R178A, R204A	C63A, R178A, R204A	C63A, R178A, R204A
β mutations	C30A	C30A	C30A, S520K
γ mutations	C33A, C41A, R138A	C33A, C41A, R138A	C33A, C41A, R1
Other treatments	—	POPC nanodisc	—
Grid Preparation			
ENaC (μM)	19.8	2	21.3
Salt	NaCl	KCl	KCl
Acid Shock	Yes	No	Yes
Fabs	α and β	—	α and β
Grid Type[1]	2/1 200	2/2 200 + 2 nm carbon	2/1 200
FOM (μM)	2	10	10
Microscopy			
Facility	PNCC	S2C2	S2C2
No. Movies	13,689	9,882	5,126
Frames[2]	50	65	50
Pixel Size (Å/pix)[3,4,5]	0.8015	0.86	0.86
Processing			
No. particles	612,591	237,730	257,341
ECD resolution (Å)[6,7]	2.34	3.06	2.94
Whole protein resolution (Å)[6,7]	2.89	—	3.26
ECD sharpening factor[6]	-56.6	-77.1	-88.9
Whole protein sharpening factor[6]	-66.0	—	-110.4
Model Building			
Starting model	6WTH	CKO digitonin	6WTH
No. non-H atoms	12,416	9,971	12,807
No. residues	1,628	1,174	1,714
No. ligands[8]	49	38	35
Bond length RMSD	0.006	0.003	0.003
Bond angle RMSD	0.709	0.505	0.519
Molprobity score	1.49	1.11	1.10
Clash score	4.61	3.14	3.06
Rama. outliers (%)	0.00	0.00	0.00
Rama. allowed (%)	2.00	1.57	1.26
Rama. favored (%)	98.00	98.43	98.74
Rotamer outliers	2.15	0.09	0.72

Cβ outliers	0.00	0.00	0.00
CaBLAM outliers	0.81	0.44	0.40
Resolution (0.143 FSC)	2.3	2.9	2.8
CC (mask)	0.85	0.84	0.83
Q-score[9]	0.80	0.71	0.71

[1]All grids are Quantifoil grids with gold mesh
[2]Electron flux is 1 e /Å^2/frame
[3]All datsets collected in super-resolution mode and Fourier-cropped back to this physical size.
[4]Resolutions here are nominal resolutions given by the microscopy facility. I have resion to believe the S^{2}C^2 pixel size is incorrect, and built the models into a corrected pixel size (see Materials and Methods).
[5]These values were used for processing and are listed to the precision given by the microscopy facility at the time of collection.
[6]A dash indicates that a focused map for this region was not used in model building
[7]GSFSC resolution
[8]NAG, MAN, and BMA. UNK is counted as a residue instead.
[9]Residues modeled as UNK excluded from Q-score

The four constructs I present here can broadly be split into those I expect to be open (CKO/DEG and mouse trypsin) and those I expect to be closed (CKO, mouse) (Table A.1). All human channels in this work have mutant furin sites (αR178A R204A and γR138A). Additionally, all human channels are ``cysteine knock-out" (CKO) mutants, with the following mutations: αC63A, βC30A, and γC33A C41A. Some (but not all) cysteines in the ENaC TMD are known to be palmitoylated[31–33]. CKO channels express at approximately eight times the yield of wild-type-like channels, with similar electrophysiological traits (Figure A.3). Mouse channels presented in this work have no mutations from the consensus gene. I expect mouse and CKO channels to be closed.

DEG channels have two mutations: βS520K and αT240W. The former mutation at what has been named the ``DEG site" holds the channel in an open state regardless of proteolytic cleavage state[34]. The DEG site sits in the TMD just above the predicted amiloride-binding site. The latter mutation in α lies in the GRIP domain and also increases the P_O of uncleaved ENaC[35].

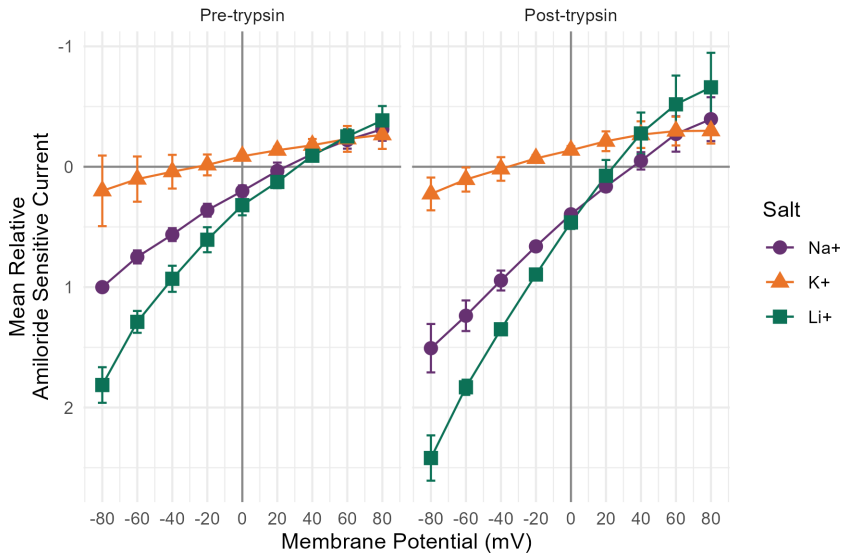

Figure A.3.: I/V curves for human CKO and CKO/DEG channels. Values are normalized per-cell to the inward current at -80 mV before trypsin treatment. Cells were treated with trypsin for five minutes before being re-recorded. Each point is the average of three cells. Error bars represent +/- one standard deviation.

A.10. Whole cell patch clamp

Human embryonic kidney cells (HEK293S/17) were grown in suspension in Freestyle medium with 10% FBS to a density of 1×10^6 cells/mL, at which point they were infected with virus carrying the appropriate ENaC genes. Cells were incubated at 37 °C overnight with 1 μM amiloride. Cells were then pipetted over a dish of DMEM plus 10% FBS with several small coverslips and allowed to adhere at 37 °C while the electrophysiology rig was prepared, approximately 2 hours. Pipettes were pulled to 2--3 MΩ resistance and filled with filtered **internal solution**

- 150 mM KCl
- 2 mM $MgCl_2$
- 5 mM EGTA
- 10 mM HEPES pH 7.4

Working one coverslip at a time, cells were moved from DMEM at 37 °C to a dish on the rig (at room temperature) containing **K^+ external solution**

- 150 mM KCl
- 2 mM $MgCl_2$
- 2 mM $CaCl_2$
- and 10 mM HEPES pH 7.4

Also prepared were solutions of Na^+ and Li^+, the same as the K^+ solution but with NaCl or LiCl replacing the KCl, respectively. Each salt solution also had a counterpart with 100 μM amiloride added. Finally, a **trypsin solution** (KCl external solution + 5 μg/mL trypsin) was prepared.

Amiloride sensitive current was determined by placing a cell in the amiloride external solution for 1 second, the amiloride-free solution for 2 seconds, and returning to the amiloride solution for 1 second. Average current during no-amiloride traces was subtracted to set the baseline to 0 A, and the maximum current during the 2 second no-amiloride duration taken as the amiloride-sensitive current. The K^+ recordings show a current spike when returning to the amiloride-containing solution, which I exclude from the calculations. This process was performed once for each holding potential between -80 and +80 mV, stepping by 20 mV. Then, this entire voltage sweep was repeated for each of the two remaining salts. The cell was then exposed to the trypsin solution for 5 minutes, and the entire set of voltage and salt sweeps repeated for the post-trypsin measurements. Thus, the full combination of voltage, salt, and proteolytic cleavage states was recorded on each cell. Once a dish

had been exposed to the trypsin solution, the dish was replaced with a fresh dish and coverslip to prevent early cleavage of unmeasured cells.